



## Article

# Analysis of Cold Composite Sheet Rolling Considering Anisotropic Effect and Position-Dependent Friction Model

Jiageng Liu <sup>1,\*</sup>, Jiang Wu <sup>2</sup>, Qian Liu <sup>3</sup>, Shuai Ji <sup>4</sup>, Xinlu Zheng <sup>1</sup>, Feng Wang <sup>1</sup>  and Jiang Wang <sup>1,\*</sup> 

<sup>1</sup> College of Materials Science and Engineering, Guilin University of Electronic Technology, Guilin 541004, China

<sup>2</sup> Zhejiang WLY Precision Manufacturing Co., Ltd., Jinhua 321000, China

<sup>3</sup> College of Metallurgy and Energy, North China University of Science and Technology, Tangshan 063210, China

<sup>4</sup> School of Materials Science and Engineering, Xi'an Shiyou University, Xi'an 710065, China

\* Correspondence: ljg@guet.edu.cn (J.L.); waj124@guet.edu.cn (J.W.)

**Abstract:** The large difference in mechanical properties and plastic deformation ability of each layer will have a great impact on the overall performance of a composite sheet prepared by cold-roll bonding. The effect of rolling and material variables on the stress distribution and bonding state in the rolling deformation zone should be studied. In this work, an accurate cold-rolling deformation model considering the anisotropic effect and position-dependent friction model is established using the slab method. Effects of different process and material variables are analyzed. Related experiments were performed on Ti-Al clads and calculation results from the deformation model were compared with the experimental results. This model can well predict the Ti/Al thickness ratio after rolling, and the smaller the initial aluminum strength, the more accurate the predicted value; the minimum error is within 1%. The deformation coordination between the titanium and aluminum layers becomes better with the increase in rolling reduction and initial aluminum strength. At 50% reduction, the deformation ratio of titanium and aluminum increases from 93.8% to 98.1%, which is consistent with the trend of the results calculated using this model.

**Keywords:** cold-rolling deformation model; anisotropic effect; position-dependent friction model; deformation coordination



**Citation:** Liu, J.; Wu, J.; Liu, Q.; Ji, S.; Zheng, X.; Wang, F.; Wang, J.

Analysis of Cold Composite Sheet Rolling Considering Anisotropic Effect and Position-Dependent Friction Model. *Metals* **2023**, *13*, 259. <https://doi.org/10.3390/met13020259>

Academic Editor: Jae Myung Lee

Received: 13 December 2022

Revised: 14 January 2023

Accepted: 21 January 2023

Published: 28 January 2023



**Copyright:** © 2023 by the authors. Licensee MDPI, Basel, Switzerland. This article is an open access article distributed under the terms and conditions of the Creative Commons Attribution (CC BY) license (<https://creativecommons.org/licenses/by/4.0/>).

## 1. Introduction

Layered metal composites are more and more widely used because of their excellent comprehensive properties compared with single metals. In addition, layered metal composites can reduce the cost of the manufacturing process or product application, so they are widely used in the aerospace, national defense and military industry, transportation and equipment manufacturing [1–7].

Rolling is the most economical and efficient method to prepare layered metal composites. The mechanical properties and plastic deformation capacity of each layer of the composite sheet are quite different. In the rolling process, the mutual restriction of each layer makes the composite sheet show different deformation behavior from the single metal as a whole. This deformation characteristic of the composite sheet makes the stress field change significantly. Meanwhile, it also affects the bonding state of the composite sheet in the deformation zone, which determines the bonding formation. Therefore, the deformation behavior of each layer in the rolling process should be comprehensively analyzed using numerical methods and theoretical models. Many researchers use the finite element method and discrete element method to analyze the deformation of composite sheets in the rolling process [7–11]. It should be mentioned here that multi-scale simulation has become more and more popular in studying the deformation behavior of sheets. Combining the

macroscopic finite element model with the atomistic modeling with anisotropic compression is useful for studying the deformation behavior and deformation coordination between layers of composite sheets. Other researchers use mathematical models to study the deformation behavior of each layer in the rolling process. These mathematical models include the upper bound method [12–14], stream function method [15], slip line method [16,17] and slab method [18,19]. Among them, the stress field cannot be obtained by the upper bound method and stream function method. Moreover, the slab method is one of the best methods to solve mechanical problems. Anisotropy effects are very important in the rolling process, but many researchers seldom consider this when establishing a deformation model using the slab method. Chaudhari et al. [20] consider the anisotropy of titanium layer when analyzing the cold-rolling deformation of a multilayer titanium/aluminum composite. Moreover, in the rolling process, different friction states exist at the interfaces of the composite sheet with the rolls and at the interface of two layers. In the theoretical and numerical analysis of rolling processes, there are usually two friction models: the Coulomb friction model and constant shear friction model. Tzou [21] proposed an analytical Coulomb model. Pan et al. [22] established an analytical model considering constant shear for the asymmetric cold and hot rolling of composites. Meanwhile, Huang et al. [23] analyzed these two friction models. The analytical results have identical trends for the two models. The relationships between the frictional coefficient and frictional factor can be obtained effectively, and the limit of the frictional coefficient generating the sticking friction is found.

Considering the extrusion process of the fresh metal at the two faying surfaces, it is known that the frictions between the composite sheet and the rolls and between the two layers are related to the position in the deformation zone. Based on this, in the analysis of the cold-rolling of a Ti/Al composite sheet, the deformation anisotropy effects of titanium and aluminum are introduced, and the position correlation of friction caused by the extrusion process of the bottom metal is also considered. In this work, the effects of rolling reduction, different initial aluminum strength, friction coefficient between titanium and aluminum and initial thickness of the aluminum layer on the stress field distribution and bonding state of the Ti/Al composite sheet during cold-rolling are analyzed and discussed, which provides a theoretical basis and related process reference for solving the problem of the poor deformation coordination and bonding performance of the composite sheet in the cold-rolling process.

## 2. Mathematical Model Formulation

In order to simplify the formulation involved in developing the analysis for cold-roll bonding of the composite sheet, the following assumptions are made [19–22]:

1. The cold-rolling process is plane-strain.
2. The roll is a rigid body.
3. The vertical stress and the horizontal stress are considered as principal stresses.
4. The friction coefficient between the titanium and roll, aluminum and roll and between titanium and aluminum varies with position at the rolling deformation zone.
5. Both Ti and Al layers satisfy the modified von Mises' criterion considering anisotropy given by  $\sigma_1 - \sigma_3 = S$  ( $S$  is the stress factor defined later in this article).

In this model, the rolling deformation zone can be divided into four regions as illustrated in Figure 1. Region I means that the hard layer is not yielded, while the soft layer is yielded. This region is located in  $x_a \leq x \leq L$  ( $L$  is the length of the deformation zone). Region II indicates that the hard layer also begins to yield, which is located in  $x_b \leq x \leq x_a$ . Region III indicates that the underlying metal is extruded from the crack and bond formation is completed, and this region is located in  $x_n \leq x \leq x_b$ . Region IV indicates that the whole composite sheet is located in the forward slip zone, which is  $0 \leq x \leq x_n$ .

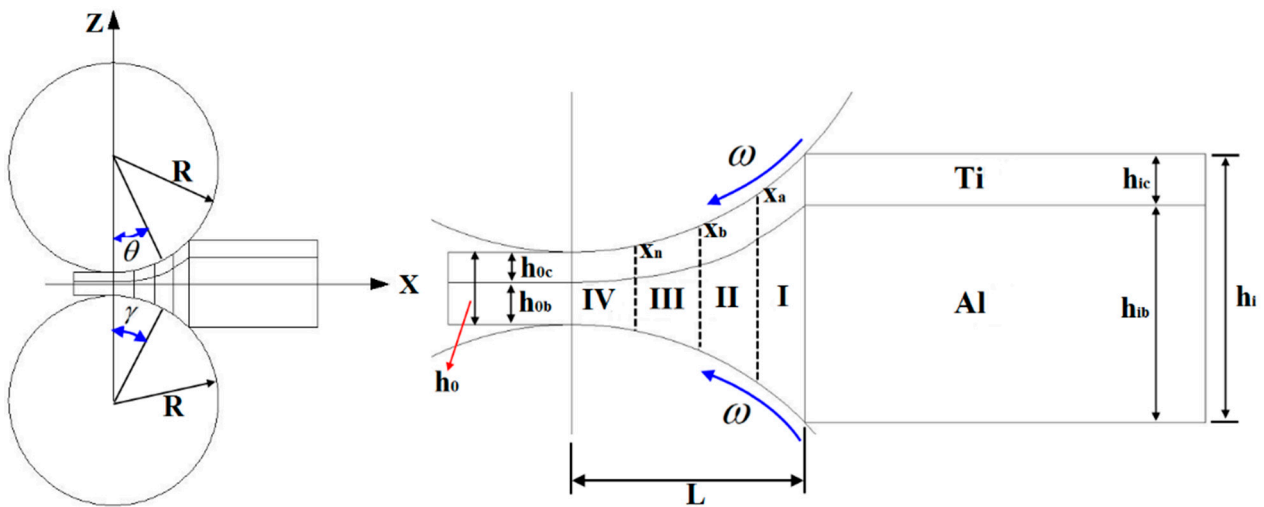


Figure 1. Schematic diagram of deformation zone of the Ti/Al composite sheet.

2.1. Region I ( $x_a \leq x \leq L$ )

The stress state of micro-element in region I is shown in Figure 2. In this region, the titanium layer does not yield, the aluminum layer yields and there is relative sliding between the titanium and aluminum layers. The aluminum layer meets the von Mises' yield criterion:  $P + \sigma_b = S_b$ ; for the titanium layer:  $P + \sigma_c < S_c$ .

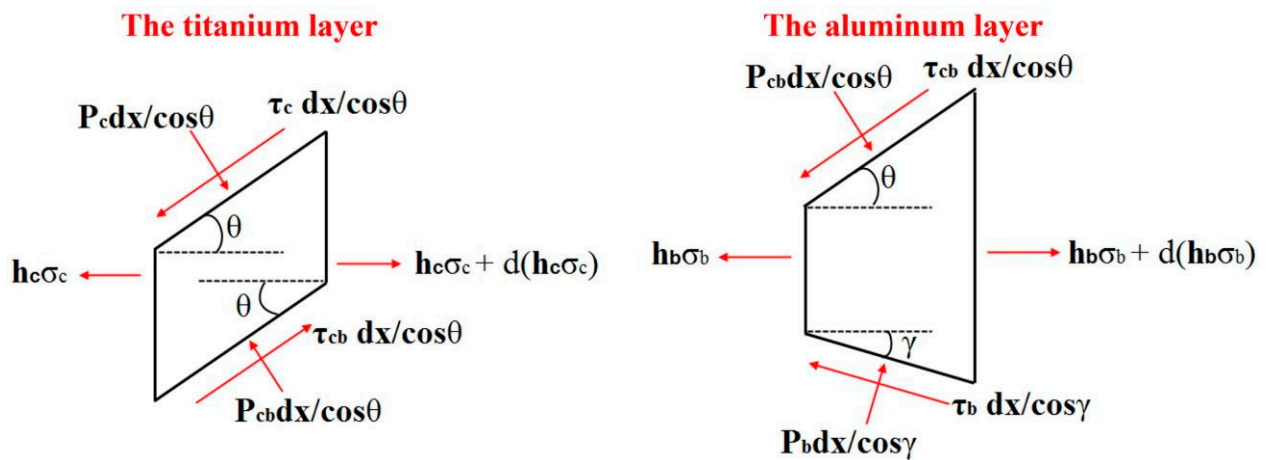


Figure 2. Stress state of micro-element in region I.

The equilibrium equation of the titanium layer in the X-direction is:

$$h_c \sigma_c + d(h_c \sigma_c) - h_c \sigma_c - \tau_c dx + P_c \tan \theta dx + \tau_{cb} dx - P_{cb} \tan \theta dx = 0 \tag{1}$$

Equation (1) can be changed as follows:

$$\frac{d(h_c \sigma_c)}{dx} + P_c \tan \theta - P_{cb} \tan \theta - \tau_c + \tau_{cb} = 0 \tag{2}$$

by the geometric relations below:

$$\begin{cases} h_c = h_{ic} \\ R(1 - \cos \theta) \approx \frac{x^2}{2R} \\ R(1 - \cos \gamma) \approx \frac{x^2}{2R} \\ h_b = h - h_c = h_0 + \frac{x^2}{R} - h_c = h_0 + \frac{x^2}{R} - h_{ic} \end{cases}$$

where  $\frac{dh_c}{dx} = 0$  and  $\tan \theta \approx \frac{x}{R}$ , so we can obtain:

$$\frac{d\sigma_c}{dx} = \frac{P_{cb} - P_c}{h_{ic}} \frac{x}{R} - \frac{\tau_c - \tau_{cb}}{h_{ic}} \quad (3)$$

The equilibrium equation of the titanium layer in the Z-direction is:

$$-P_c dx - \tau_c \tan \theta dx + P_{cb} dx + \tau_{cb} \tan \theta dx = 0 \quad (4)$$

Equation (4) can be changed as follows:

$P = P_c + \tau_c \tan \theta = P_{cb} + \tau_{cb} \tan \theta$ , which can be brought into Equation (3) to obtain:

$$\frac{d\sigma_c}{dx} = \frac{\tau_c - \tau_{cb}}{h_{ic}} \left( \frac{x^2}{R^2} + 1 \right) \quad (5)$$

The equilibrium equation of the aluminum layer in the X-direction is:

$$h_b \sigma_b + d(h_b \sigma_b) - h_b \sigma_b + P_{cb} \tan \theta dx - \tau_{cb} dx + P_b \tan \gamma dx - \tau_b dx = 0 \quad (6)$$

Equation (6) can be changed as follows:

$$\frac{d(h_b \sigma_b)}{dx} = \tau_{cb} + \tau_b - P_{cb} \tan \theta - P_b \tan \gamma \quad (7)$$

where  $\frac{dh_b}{dx} = \frac{dh}{dx} = \tan \theta + \tan \gamma = \frac{2x}{R}$ . Equation (7) can also be written as:

$$\left( h_0 + \frac{x^2}{R} - h_{ic} \right) \frac{d\sigma_b}{dx} = -\sigma_b \frac{2x}{R} + \tau_{cb} + \tau_b - (P_{cb} + P_b) \frac{x}{R} \quad (8)$$

The equilibrium equation of the aluminum layer in the Z-direction is:

$$-P_{cb} dx - \tau_{cb} \tan \theta dx + P_b dx + \tau_b \tan \gamma = 0 \quad (9)$$

Equation (9) can be changed as follows:

$P = P_{cb} + \tau_{cb} \tan \theta = P_b + \tau_b \tan \gamma$ , which can be brought into Equation (8) to obtain:

$$\frac{dP}{dx} = \frac{2S_b x}{(h_0 - h_{ic})R + x^2} - (\tau_{cb} + \tau_b) \frac{R^2 + x^2}{(h_0 - h_{ic})R^2 + Rx^2} \quad (10)$$

## 2.2. Region II ( $x_b \leq x \leq x_a$ )

The stress state of micro-element in region II is shown in Figure 3. In this region, both the titanium and aluminum layers yield, satisfying the following relationships:  $P + \sigma_b = S_b$  and  $P + \sigma_c = S_c$ . At  $x = x_b$ , the extruded metals are in contact with each other, but the bond formation is not completed, and the Ti/Al thickness ratio remains unchanged.

The equilibrium equation of the titanium layer in the X-direction is:

$$h_c \sigma_c + d(h_c \sigma_c) - h_c \sigma_c - \tau_c dx + P_c \tan \theta dx - P_{cb} \tan \theta' + \tau_{cb} dx = 0 \quad (11)$$

Equation (11) can be changed as follows:

$$\frac{d(h_c \sigma_c)}{dx} + P_c \tan \theta - P_{cb} \tan \theta' - \tau_c + \tau_{cb} = 0 \quad (12)$$

where  $\frac{dh_c}{dx} = \tan \theta - \tan \theta'$ , and

$$\frac{dh_c}{dx} = \frac{h_c}{h} \frac{dh}{dx} = \eta(\tan \theta + \tan \gamma) \quad (13)$$

So, we can obtain:

$$\tan \theta' = (1 - \eta) \tan \theta - \eta \tan \gamma = (1 - 2\eta) \frac{x}{R} = \left(1 - \frac{2h_{ic}}{h_0 + \frac{x_a^2}{R}}\right) \frac{x}{R} \tag{14}$$

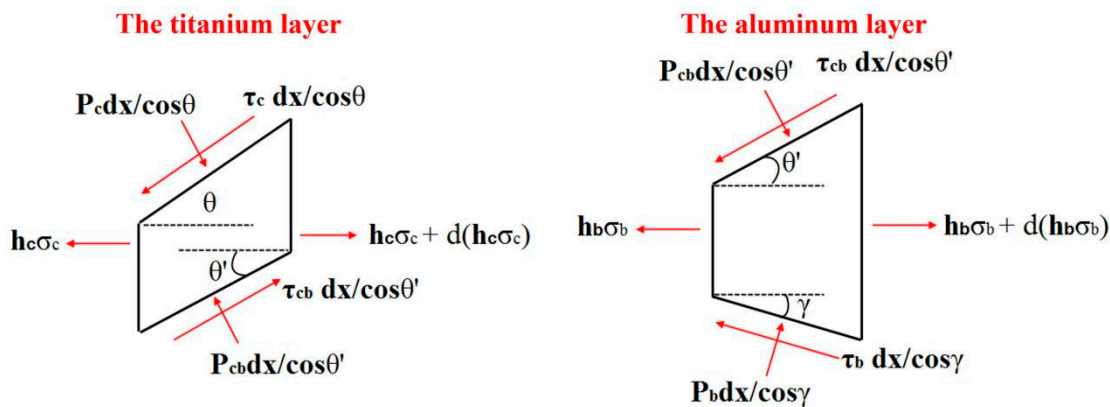


Figure 3. Stress state of micro-element in region II.

The equilibrium equation of the titanium layer in the Z-direction is:

$$- P_c dx - \tau_c \tan \theta dx + P_{cb} dx + \tau_{cb} \tan \theta' dx = 0 \tag{15}$$

Equation (15) can be changed as follows:

$P = P_c + \tau_c \tan \theta = P_{cb} + \tau_{cb} \tan \theta'$ . By introducing this equation and Equation (14) into Equation (12), we can obtain:

$$\frac{dP}{dx} = \frac{2S_c x}{R \left(h_0 + \frac{x^2}{R}\right)} - \frac{\tau_c \left(\frac{x^2}{R^2} + 1\right)}{\eta \left(h_0 + \frac{x^2}{R}\right)} + \frac{\tau_{cb} \left[(1 - 2\eta)^2 \frac{x^2}{R^2} + 1\right]}{\eta \left(h_0 + \frac{x^2}{R}\right)} \tag{16}$$

The equilibrium equation of the aluminum layer in the X-direction is:

$$h_b \sigma_b + d(h_b \sigma_b) - h_b \sigma_b + P_{cb} \tan \theta' dx - \tau_{cb} dx + P_b \tan \gamma dx - \tau_b dx = 0 \tag{17}$$

Equation (17) can be changed as follows:

$$\frac{d(h_b \sigma_b)}{dx} + P_{cb} \tan \theta' + P_b \tan \gamma - \tau_{cb} - \tau_b = 0 \tag{18}$$

where  $h_b = (1 - \eta)h$ , and we can obtain:

$$\frac{dh_b}{dx} = (1 - \eta) \frac{dh}{dx} = (1 - \eta)(\tan \theta + \tan \gamma) \tag{19}$$

The equilibrium equation of the aluminum layer in the Z-direction is:

$$- P_{cb} dx - \tau_{cb} \tan \theta' dx + P_b dx + \tau_b \tan \gamma dx = 0 \tag{20}$$

Equation (20) can be changed as follows:

$P = P_{cb} + \tau_{cb} \tan \theta' = P_b + \tau_b \tan \gamma$ . By introducing this equation and Equation (19) into Equation (18), we can obtain:

$$\frac{dP}{dx} = \frac{2S_b x}{R \left(h_0 + \frac{x^2}{R}\right)} - \frac{\tau_{cb} \left[1 + (1 - 2\eta)^2 \frac{x^2}{R^2}\right]}{(1 - \eta) \left(h_0 + \frac{x^2}{R}\right)} - \frac{\tau_b \left(1 + \frac{x^2}{R^2}\right)}{(1 - \eta) \left(h_0 + \frac{x^2}{R}\right)} \tag{21}$$

2.3. Region III ( $x_n \leq x \leq x_b$ )

The stress state of micro-element in region III is shown in Figure 4. In this region, at  $x = x_b$ , the joining occurs when the base metal extrudes from the crack and, subsequently, the titanium and aluminum layers are deformed as a single unit;  $P + \sigma = \eta S_c + (1 - \eta) S_b$ .

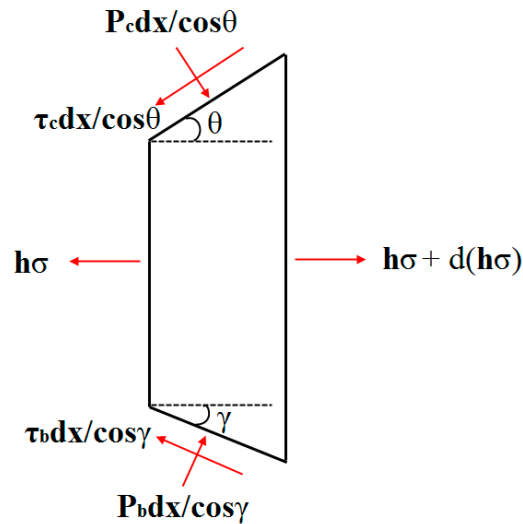


Figure 4. Stress state of micro-element in region III.

The equilibrium equation for the composite sheet in the X-direction is:

$$h\sigma + d(h\sigma) - h\sigma + P_c \tan \theta dx - \tau_c dx + P_b \tan \gamma dx - \tau_b dx = 0 \tag{22}$$

Equation (22) can be changed as follows:

$$\left( h_0 + \frac{x^2}{R} \right) \frac{d\sigma}{dx} + \frac{2\sigma x}{R} + (P_c + P_b) \frac{x}{R} - (\tau_c + \tau_b) = 0 \tag{23}$$

The equilibrium equation for the composite sheet in the Z-direction is:

$$- P_c dx - \tau_c \tan \theta dx + P_b dx + \tau_b \tan \gamma dx = 0 \tag{24}$$

Equation (24) can be changed as follows:

$P = P_c + \tau_c \tan \theta = P_b + \tau_b \tan \gamma$ . By introducing this equation into Equation (23), we can obtain:

$$\frac{dP}{dx} = \frac{2[\eta S_c + (1 - \eta) S_b] x}{R h_0 + x^2} - \frac{\left( 1 + \frac{x^2}{R^2} \right) (\tau_c + \tau_b)}{h_0 + \frac{x^2}{R}} \tag{25}$$

2.4. Region IV ( $0 \leq x \leq x_n$ )

The stress state of micro-element in region IV is shown in Figure 5. In this region, the friction between the composite sheet and the upper and lower rolls is reversed, and the composite sheet as a whole enters the forward slip zone.

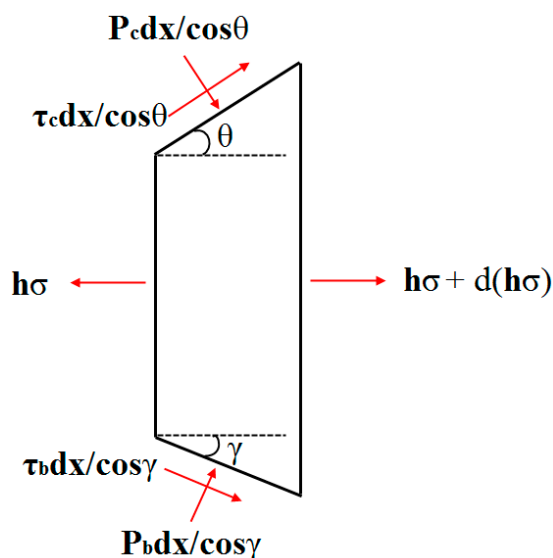


Figure 5. Stress state of micro-element in region IV.

The equilibrium equation for the composite sheet in the X-direction is:

$$h\sigma + d(h\sigma) - h\sigma + P_c \tan \theta dx + \tau_c dx + P_b \tan \gamma dx + \tau_b dx = 0 \tag{26}$$

Equation (26) can be changed as follows:

$$\left( h_0 + \frac{x^2}{R} \right) \frac{d\sigma}{dx} + \frac{2\sigma x}{R} + (P_c + P_b) \frac{x}{R} + (\tau_c + \tau_b) = 0 \tag{27}$$

The equilibrium equation for the composite sheet in the Z-direction is:

$$- P_c dx + \tau_c \tan \theta dx + P_b dx - \tau_b \tan \gamma dx = 0 \tag{28}$$

Rectification gives:  $P = P_c - \tau_c \tan \theta = P_b - \tau_b \tan \gamma$ , which, when taken into Equation (27), gives:

$$\frac{dP}{dx} = \frac{2[\eta S_c + (1 - \eta) S_b] x}{R h_0 + x^2} + \frac{\left( 1 + \frac{x^2}{R^2} \right) (\tau_c + \tau_b)}{h_0 + \frac{x^2}{R}} \tag{29}$$

### 2.5. Definition of the Coefficient of Friction

Because of the brittleness and inextensibility of the covering layer, the friction coefficients between the surfaces depend on the surface extension deformation. The average friction coefficients  $\bar{\mu}_c$  between the roll and the titanium layer,  $\bar{\mu}_{cb}$  between the titanium layer and the aluminum layer and  $\bar{\mu}_b$  between the roll and the aluminum layer are defined in the following [24]:

$$\begin{cases} \bar{\mu}_c = \mu_c(1 - h_{t,J}) + \mu'_{c,t,J} h_{t,J} = \mu_c + (\mu'_{c,t,J} - \mu_c) h_{t,J} \\ \bar{\mu}_{cb} = \mu_{cb}(1 - h_{t,J}) + \mu'_{cb,t,J} h_{t,J} = \mu_{cb} + (\mu'_{cb,t,J} - \mu_{cb}) h_{t,J} \\ \bar{\mu}_b = \mu_b(1 - h_{t,J}) + \mu'_{b,t,J} h_{t,J} = \mu_b + (\mu'_{b,t,J} - \mu_b) h_{t,J} \end{cases} \tag{30}$$

Here,  $\mu_c$  is the friction coefficient between the roll surface and the covering layer on the surface of the titanium,  $\mu_{cb}$  is the friction coefficient between the covering layer on the surface of the titanium and the covering layer on the surface of the aluminum and  $\mu_b$  is the friction coefficient between the roll surface and the covering layer on the surface of the aluminum.  $\mu'_{c,t,J}$ ,  $\mu'_{cb,t,J}$  and  $\mu'_{b,t,J}$  are the friction coefficients (between the rolls and the facing surfaces of the titanium layer, between the rolls and the facing surfaces

of the aluminum layer and between the titanium and aluminum layers) in the crevice section between covering layer fragments. When the crevice is small, the extruded metal does not contact the facing surface of the other metal sheet and, thus,  $\mu'_c = 0, \mu'_{cb} = 0, \mu'_b = 0$ . Once the extruded metal goes through the crevice and contacts the other surface, the friction coefficients are  $\mu'_c = 1, \mu'_{cb} = 1$  and  $\mu'_b = 1$ .  $h_{t,J}(x)$  denotes the overall reduction in the composite sheet at position  $x$  in region  $J$  ( $J = I, II, III, IV$ ), thus  $h_{t,J}(x) = 1 - \frac{Rh_0 + x^2}{Rh_i}$ . Therefore, the average friction stress becomes:

In region I,

$$\begin{cases} \tau_c = (\mu_c + (\mu'_c - \mu_c)h_{t,I})S_c \\ \tau_{cb} = (\mu_{cb} + (\mu'_{cb} - \mu_{cb})h_{t,I})S_b \\ \tau_b = (\mu_b + (\mu'_b - \mu_b)h_{t,I})S_b \end{cases} \tag{31}$$

In region II,

$$\begin{cases} \tau_c = (\mu_c + (\mu'_c - \mu_c)h_{t,II})S_c \\ \tau_{cb} = (\mu_{cb} + (\mu'_{cb} - \mu_{cb})h_{t,II})S_b \\ \tau_b = (\mu_b + (\mu'_b - \mu_b)h_{t,II})S_b \end{cases} \tag{32}$$

In region III,

$$\begin{cases} \tau_c = (\mu_c + (\mu'_c - \mu_c)h_{t,III})(\eta S_c + (1 - \eta)S_b) \\ \tau_b = (\mu_b + (\mu'_b - \mu_b)h_{t,III})(\eta S_c + (1 - \eta)S_b) \end{cases} \tag{33}$$

In region IV,

$$\begin{cases} \tau_c = (\mu_c + (\mu'_c - \mu_c)h_{t,IV})(\eta S_c + (1 - \eta)S_b) \\ \tau_b = (\mu_b + (\mu'_b - \mu_b)h_{t,IV})(\eta S_c + (1 - \eta)S_b) \end{cases} \tag{34}$$

### 2.6. Solving for Stresses in Each Region

Let  $\sigma_{c,J}, P_{c,J}, \sigma_{b,J}$  and  $P_{b,J}$  denote the horizontal and vertical stresses in the titanium layer and the horizontal and vertical stresses in the aluminum layer in region  $J$  ( $J = I, II$ ), respectively.  $P_{III}$  and  $P_{IV}$  are the vertical stresses in the composite sheet in regions III and IV, respectively.

In region I,

$$\sigma_{c,I} = A_{I,\sigma_c}x + \frac{1}{3}\left(B_{I,\sigma_c} + \frac{A_{I,\sigma_c}}{R^2}\right)x^3 + \frac{B_{I,\sigma_c}}{5R^2}x^5 + C_{I,\sigma_c} \tag{35}$$

where  $A_{I,\sigma_c} = \frac{S_c\mu'_c - S_b\mu'_{cb} - \frac{S_ch_0(\mu'_c - \mu_c)}{h_i} + \frac{S_bh_0(\mu'_{cb} - \mu_{cb})}{h_i}}{h_{ic}}$ ,  $B_{I,\sigma_c} = \frac{S_b(\mu'_{cb} - \mu_{cb}) - S_c(\mu'_c - \mu_c)}{Rh_i h_{ic}}$ ;

From  $\sigma_{c,I} = 0$  at  $x = L$ , the integration constant can be obtained:

$$C_{I,\sigma_c} = -A_{I,\sigma_c}L - \frac{1}{3}\left(B_{I,\sigma_c} + \frac{A_{I,\sigma_c}}{R^2}\right)L^3 - \frac{B_{I,\sigma_c}}{5R^2}L^5.$$

$$\begin{aligned} P_{b,I} &= \frac{B_{I,P_b}x^3}{3R} - \left(B_{I,P_b}(h_0 - h_{ic}) - RB_{I,P_b} + \frac{A_{I,P_b}}{R}\right)x + S_b \ln(x^2 + (h_0 - h_{ic})R) \\ &+ \frac{\arctan\left(\frac{x}{\sqrt{R(h_0 - h_{ic})}}\right)}{\sqrt{R(h_0 - h_{ic})}} \left(B_{I,P_b}R(h_0 - h_{ic})^2 - (B_{I,P_b}R^2 - A)(h_0 - h_{ic}) - RA_{I,P_b}\right) + C_{I,P_b} \end{aligned} \tag{36}$$

where  $A_{I,P_b} = S_b(\mu'_{cb} + \mu'_b) - \frac{S_bh_0}{h_i} \left[ (\mu'_{cb} - \mu_{cb}) + (\mu'_b - \mu_b) \right]$ ,  $B_{I,P_b} = \frac{S_b}{Rh_i} \left[ (\mu'_{cb} - \mu_{cb}) + (\mu'_b - \mu_b) \right]$ ;



From  $\sigma_{b,I} = 0$  at  $x = L$ , and  $\sigma_{b,I} + P_{b,I} = S_b$ , the integration constant can be obtained:

$$C_{I,P_b} = S_b - \frac{B_{I,P_b} L^3}{3R} + \left( B_{I,P_b} (h_0 - h_{ic}) - R B_{I,P_b} + \frac{A_{I,P_b}}{R} \right) L - S_b \ln(L^2 + (h_0 - h_{ic})R) - \frac{\arctan\left(\frac{L}{\sqrt{R(h_0 - h_{ic})}}\right)}{\sqrt{R(h_0 - h_{ic})}} \left( B_{I,P_b} R (h_0 - h_{ic})^2 - (B_{I,P_b} R^2 - A) (h_0 - h_{ic}) - R A_{I,P_b} \right)$$

We can find  $x_a$  by  $\sigma_{c,I} + P_{b,I} = S_c$ , using the dichotomy method.

In region II,

$$P_{c,II} = \frac{-D_{II,P_c} h_0 R^2 + B_{II,P_c} R}{\eta} x + \frac{D_{II,P_c} R}{3\eta} x^3 + S_c \ln(h_0 R + x^2) + \frac{\arctan\left(\frac{x}{\sqrt{R h_0}}\right)}{\eta \sqrt{R h_0}} \left( D_{II,P_c} h_0^2 R^3 - B_{II,P_c} h_0 R^2 + A_{II,P_c} R \right) + C_{II,P_c} \quad (37)$$

where

$$A_{II,P_c} = \mu'_{cb} S_b - S_c \mu'_c + \frac{S_c h_0}{h_i} (\mu'_c - \mu_c) - \frac{h_0 S_b}{h_i} (\mu'_{cb} - \mu_{cb}),$$

$$B_{II,P_c} = -\frac{\mu'_c S_c}{R^2} + \frac{\mu'_{cb} (1-2\eta)^2 S_b}{R^2} + \frac{S_c (\mu'_c - \mu_c)}{R h_i} - \frac{\mu'_{cb} - \mu_{cb}}{R h_i} S_b + \frac{S_c h_0}{R^2 h_i} (\mu'_c - \mu_c) - \frac{h_0 (1-2\eta)^2 (\mu'_{cb} - \mu_{cb})}{R^2 h_i} S_b,$$

$$D_{II,P_c} = \frac{S_c (\mu'_c - \mu_c)}{R^3 h_i} - \frac{(1-2\eta)^2 (\mu'_{cb} - \mu_{cb})}{R^3 h_i} S_b.$$

$$P_{b,II} = \frac{D_{II,P_b} h_0 R^2 + B_{II,P_b} R}{\eta - 1} x - \frac{D_{II,P_b} R}{3(\eta - 1)} x^3 + S_b \ln(h_0 R + x^2) - \frac{\arctan\left(\frac{x}{\sqrt{R h_0}}\right)}{(\eta - 1) \sqrt{R h_0}} \left( D_{II,P_b} h_0^2 R^3 + B_{II,P_b} h_0 R^2 - A_{II,P_b} R \right) + C_{II,P_b} \quad (38)$$

where

$$A_{II,P_b} = S_b \left( \mu'_{cb} - (\mu'_{cb} - \mu_{cb}) \frac{h_0}{h_i} \right) + S_b \left( \mu'_b - (\mu'_b - \mu_b) \frac{h_0}{h_i} \right),$$

$$B_{II,P_b} = S_b \left( (1-2\eta)^2 \left( \mu'_{cb} - (\mu'_{cb} - \mu_{cb}) \frac{h_0}{h_i} \right) \frac{1}{R^2} - \frac{\mu'_{cb} - \mu_{cb}}{R h_i} \right) + S_b \left( \frac{1}{R^2} \left( \mu'_b - (\mu'_b - \mu_b) \frac{h_0}{h_i} \right) - \frac{\mu'_b - \mu_b}{R h_i} \right),$$

$$D_{II,P_b} = \frac{S_b (\mu'_{cb} - \mu_{cb}) (1-2\eta)^2}{R^3 h_i} + \frac{S_b (\mu'_b - \mu_b)}{R^3 h_i}.$$

From  $P_{b,I}|_{x=x_a} = P_{b,II}|_{x=x_a}$ , we can find  $C_{II,P_b}$ .

In region III,

$$P_{III} = -(D_{III} h_0 R^2 + B_{III} R) x + \frac{1}{3} D_{III} R x^3 + (\eta S_c + (1 - \eta) S_b) \ln(h_0 R + x^2) + \frac{\arctan\left(\frac{x}{\sqrt{R h_0}}\right)}{\sqrt{R h_0}} \left( D_{III} h_0^2 R^3 + B_{III} h_0 R^2 - A_{III} R \right) + C_{III} \quad (39)$$

where

$$A_{III} = (\eta S_c + (1 - \eta) S_b) \left[ (\mu'_c + \mu'_b) - \frac{h_0}{h_i} \left( (\mu'_c - \mu_c) + (\mu'_b - \mu_b) \right) \right],$$

$$B_{III} = (\eta S_c + (1 - \eta) S_b) \left\{ \frac{(\mu'_c + \mu'_b) - \frac{h_0}{h_i} [(\mu'_c - \mu_c) + (\mu'_b - \mu_b)]}{R^2} - \left( \frac{(\mu'_c - \mu_c)}{R h_i} + \frac{(\mu'_b - \mu_b)}{R h_i} \right) \right\},$$

$$D_{III} = \frac{\eta S_c + (1 - \eta) S_b}{R^2} \left( \frac{(\mu'_c - \mu_c)}{R h_i} + \frac{(\mu'_b - \mu_b)}{R h_i} \right).$$

In region IV,

$$P_{IV} = (D_{IV} h_0 R^2 + B_{IV} R) x - \frac{1}{3} D_{IV} R x^3 + (\eta S_c + (1 - \eta) S_b) \ln(h_0 R + x^2) - \frac{\arctan\left(\frac{x}{\sqrt{R h_0}}\right)}{\sqrt{R h_0}} \left( D_{IV} h_0^2 R^3 + B_{IV} h_0 R^2 - A_{IV} R \right) + C_{IV} \quad (40)$$

where

$$A_{IV} = (\eta S_c + (1 - \eta) S_b) \left[ (\mu'_c + \mu'_b) - \frac{h_0}{h_i} \left( (\mu'_c - \mu_c) + (\mu'_b - \mu_b) \right) \right],$$

$$B_{IV} = (\eta S_c + (1 - \eta) S_b) \left\{ \frac{(\mu'_c + \mu'_b) - \frac{h_0}{h_i} [(\mu'_c - \mu_c) + (\mu'_b - \mu_b)]}{R^2} - \left( \frac{(\mu'_c - \mu_c)}{R h_i} + \frac{(\mu'_b - \mu_b)}{R h_i} \right) \right\},$$

$$D_{IV} = \frac{\eta S_c + (1 - \eta) S_b}{R^2} \left( \frac{(\mu'_c - \mu_c)}{R h_i} + \frac{(\mu'_b - \mu_b)}{R h_i} \right).$$

At  $x = 0, \sigma_{IV} = 0$ . From  $P_{IV} + \sigma_{IV} = \eta S_c + (1 - \eta) S_b$ , we can find  $C_{IV}$ . Using  $P_{III} = P_{IV}$ , we can find  $x_n$  using dichotomy.

The relationship between  $x_b$  and  $x_n$  can be established according to the principle of volume invariance [22], and from  $V_b h_b = V_n h_n$ , it follows that  $x_b = \sqrt{Rh_0(V-1) + Vx_n^2}$ , where  $V_b$  and  $V_n$  are the velocities of the Ti/Al composite sheet when it passes through positions  $x_b$  and  $x_n$ , respectively.

Therefore, we can summarize the solution process in Figure 6 as follows:

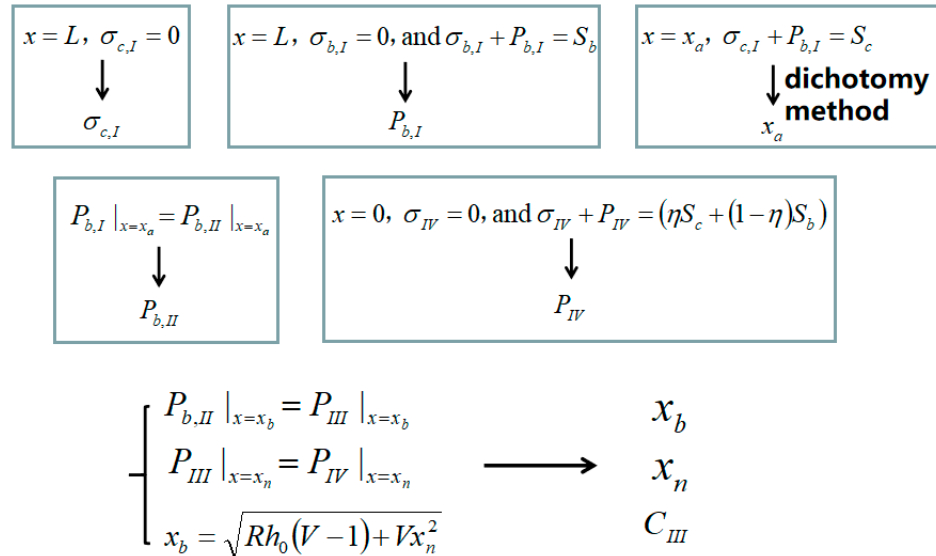


Figure 6. Solution diagram of  $x_b$ ,  $x_n$  and  $C_{III}$ .

2.7. Determination of the Anisotropic Yielding Criterion and Parameters for Each Layer

The deformation model considers the anisotropy of the Ti and Al layers. In order to describe the yielding behavior of orthotropic plastic anisotropic materials, Hill [25] proposed a mathematical description of plastic anisotropy, stating that if the yield criterion is quadratic in the stress component, it must have the following form:

$$2f(\sigma_{ij}) = F(\sigma_y - \sigma_z)^2 + G(\sigma_z - \sigma_x)^2 + H(\sigma_x - \sigma_y)^2 + 2L\tau_{yz}^2 + 2M\tau_{zx}^2 + 2N\tau_{xy}^2 = 1 \quad (41)$$

where  $F, G, H, L, M$  and  $N$  are the characteristic parameters of the instantaneous anisotropic state. When the anisotropic yielding principal axis is the reference axis, the anisotropic yielding function has the following form:

$$2f(\sigma_{ij}) = F(\sigma_2 - \sigma_3)^2 + G(\sigma_3 - \sigma_1)^2 + H(\sigma_1 - \sigma_2)^2 = 1 \quad (42)$$

where  $x, y$  and  $z$  are replaced by the principal stress directions 1, 2 and 3, and such that 1, 2 and 3 denote the rolling direction, transverse direction and normal direction, respectively. If  $X, Y$  and  $Z$  are the tensile yield stresses in the anisotropic principal directions, then it follows that:

$$\begin{cases} \frac{1}{X^2} = G + H, 2F = \frac{1}{Y^2} + \frac{1}{Z^2} - \frac{1}{X^2} \\ \frac{1}{Y^2} = H + F, 2G = \frac{1}{Z^2} + \frac{1}{X^2} - \frac{1}{Y^2} \\ \frac{1}{Z^2} = F + G, 2H = \frac{1}{X^2} + \frac{1}{Y^2} - \frac{1}{Z^2} \end{cases} \quad (43)$$

Hill gives the strain increment relationship in the anisotropic principal axis direction as:

$$\begin{cases} d\varepsilon_1 = d\lambda[H(\sigma_1 - \sigma_2) + G(\sigma_1 - \sigma_3)] \\ d\varepsilon_2 = d\lambda[F(\sigma_2 - \sigma_3) + H(\sigma_2 - \sigma_1)] \\ d\varepsilon_3 = d\lambda[G(\sigma_3 - \sigma_1) + F(\sigma_3 - \sigma_2)] \end{cases} \quad (44)$$

Since rolling is a plane-strain process,  $\sigma_2 = \frac{F\sigma_3 + H\sigma_1}{F+H}$  can be obtained from  $d\varepsilon_2 = 0$ . Bringing in Equation (42), we have  $\left(G + \frac{FH}{F+H}\right)(\sigma_1 - \sigma_3)^2 = 1$ . Therefore, from  $\sigma_1 - \sigma_3 = S$ , the following equation is obtained:

$$S = \left(G + \frac{FH}{F+H}\right)^{-1/2} = \left[\frac{1}{2}\left(\frac{1}{Z^2} + \frac{1}{X^2} - \frac{1}{2Y^2}\right) + \frac{Y^2}{2}\left(\frac{1}{X^2Z^2} - \frac{1}{2Z^4} - \frac{1}{2X^4}\right)\right]^{-1/2} \quad (45)$$

Due to the thinness of the Ti and Al layers, the tensile yield stress along the thickness direction cannot be measured, so it can be calculated indirectly through tensile tests along the rolling and transverse directions [20]. Plate-type tensile specimens (gage length: 25 mm, gage width: 6 mm) were prepared in the rolling and transverse directions.  $Z$  can be expressed by the following equation:

$$Z = X\sqrt{T(1+M)/(T+M)} \quad (46)$$

where  $M = \frac{d\varepsilon_2}{d\varepsilon_3} = \frac{-d\varepsilon_2}{-(d\varepsilon_1+d\varepsilon_2)} = \ln\left(\frac{w_0}{w}\right) / \ln\left(\frac{wl}{w_0l_0}\right)$  indicates the strain ratio along the transverse and thickness directions in the tensile test of the specimen sampled along the rolling direction.  $T = R_{90} = \frac{d\varepsilon_1}{d\varepsilon_3} = \ln\left(\frac{w_0}{w}\right) / \ln\left(\frac{wl}{w_0l_0}\right)$  indicates the strain ratio along the transverse and thickness directions in a tensile test of a specimen taken along the transverse direction, as shown in Figure 7.  $w$  and  $l$  are the width and length of the specimen during the tension test, and  $\varepsilon_w$  and  $\varepsilon_t$  indicate the strain along the width and thickness directions.

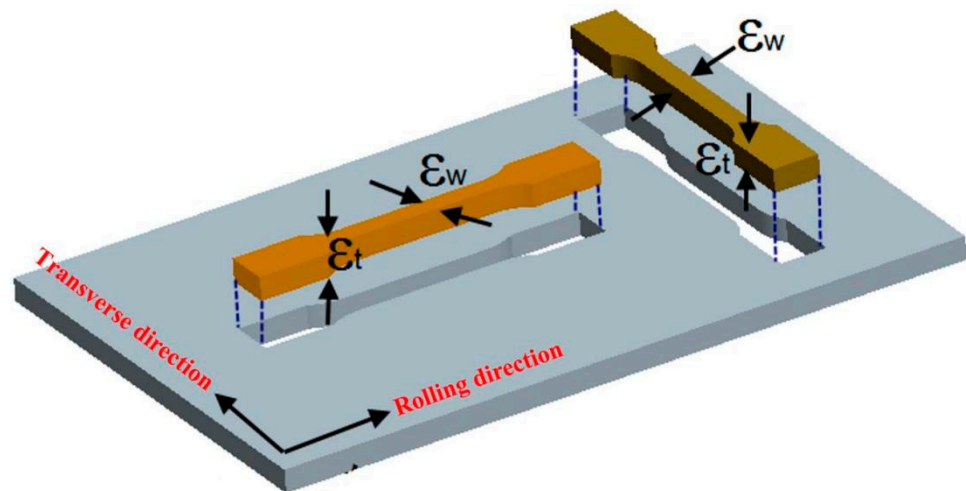


Figure 7. The tensile specimen cut from raw material.

### 3. Results and Discussion

The three characteristic points in the cold-rolled deformation model proposed in this work divide the deformation zone into four regions.  $x_a$ ,  $x_b$  and  $x_n$  represent the starting point of the yielding of the titanium layer, the point at which extrusion of fresh metal from the faying surfaces comes into contact (i.e., the bonding point) and the point where the velocity direction of the composite sheet changes (i.e., the neutral point). The composite sheet has different stress states in different regions, which are related to the yield state of the titanium layer, the rupture of the covering layers on the faying surfaces and the extrusion of the underlying fresh metal, and the speed of the composite sheet with respect to the rolls. In order to investigate the effect of titanium layer yielding, covering layer rupture and metal flow, and composite sheet speed on the stress distribution and bonding state in the deformation zone, the ratios of the position of three characteristic points relative to the length of the deformation zone (contact arc length) were introduced, namely  $x_a/L$ ,  $x_b/L$  and  $x_n/L$ .

### 3.1. Verification of Model Reliability

In order to verify the accuracy of the model, a Ti/Al cold-rolled experiment was carried out to examine the post-rolled Ti/Al thickness ratio as a target for comparison with the model's predicted values. Three types of AA4047 aluminum alloys with different strengths were obtained by the following treatment: AA4047 aluminum alloy with a thickness of 2.0 mm was rolled to 1.2 mm in two passes (2.0 mm→1.5 mm→1.2 mm); part of this rolled alloy was annealed at 300 °C for 1 h; AA4047 aluminum alloy with a thickness of 5.0 mm was rolled to 1.2 mm in four passes (5 mm→3.5 mm→2 mm→1.5 mm→1.2 mm). The AA4047 aluminum alloys after the annealing treatment, two-pass strengthening treatment and four-pass strengthening treatment are expressed as Al ①, Al ② and Al ③, respectively. According to the definition of R and P, we conducted corresponding tensile tests to determine these two parameters. All clad sheets with the stacking sequences of TA1/AA4047 were cold-rolled by one pass. The parameters in the cold-roll bonding model are listed in Tables 1 and 2. Here, S1, S2 and S3 denote the Ti/Al composite sheets obtained by cold-rolling titanium with Al ①, Al ② and Al ③, respectively, and other parameters are shown in Table 3.

**Table 1.** Plastic anisotropy coefficients  $M$  and  $T$  of titanium and aluminum.

Plastic Anisotropy Coefficient	Al ①	Al ②	Al ③	Ti
$M$	0.44	0.57	0.63	1.96
$T$	0.53	0.60	0.57	4.12

**Table 2.** Other parameters in cold-roll bonding model.

$\mu_c$	$\mu_b$	$\mu_{cb}$	Roll Radius (R)	Thickness of Aluminum Layer before Rolling ( $h_{ib}$ )	$V$	Thickness of Titanium Layer before Rolling ( $h_{ic}$ )	Yield Stress of Aluminum in Rolling Direction	Yield Stress of Aluminum in Transverse Direction
0.2	0.3	0.2	135 mm	0.6 mm	1.1	0.2 mm	43.6 MPa	43.6 MPa
		0.4		1.2 mm		0.4 mm	98.0 MPa	94.0 MPa
		0.6		1.8 mm		0.6 mm	279.0 MPa	258.0 MPa

The yield stresses of titanium layer in rolling and transverse directions are both 229.4 MPa. The yield stresses of aluminum layer in rolling and transverse directions are both 43.6 MPa, and this state of aluminum corresponds to Al ①. The yield stresses of aluminum layer in rolling and transverse directions are 98 MPa and 94 MPa, and this state of aluminum corresponds to Al ②. The yield stresses of aluminum layer in rolling and transverse directions are 279 MPa and 258 MPa, and this state of aluminum corresponds to Al ③.

**Table 3.** Cold-rolling experimental parameters for model verification.

$\mu_c$	$\mu_b$	$\mu_{cb}$	Roll Radius (R)	Thickness of Aluminum Layer before Rolling ( $h_{ib}$ )	$V$	Thickness of Titanium Layer before Rolling ( $h_{ic}$ )	Rolling Reduction
0.2	0.3	0.4	135 mm	1.2 mm	1.1	0.2 mm	35%, 42%, 50%

The Ti/Al thickness ratio values measured using the theoretical model and experiments are given in Figure 8. It can be seen that, for the case of low aluminum strength, the error between the theoretical model and the actual measured values is small, and the minimum error is within 1%. When the aluminum strength increases, the error will expand to a certain extent, but the maximum error is not more than 10%. It can be shown that the theoretical model has certain reliability.

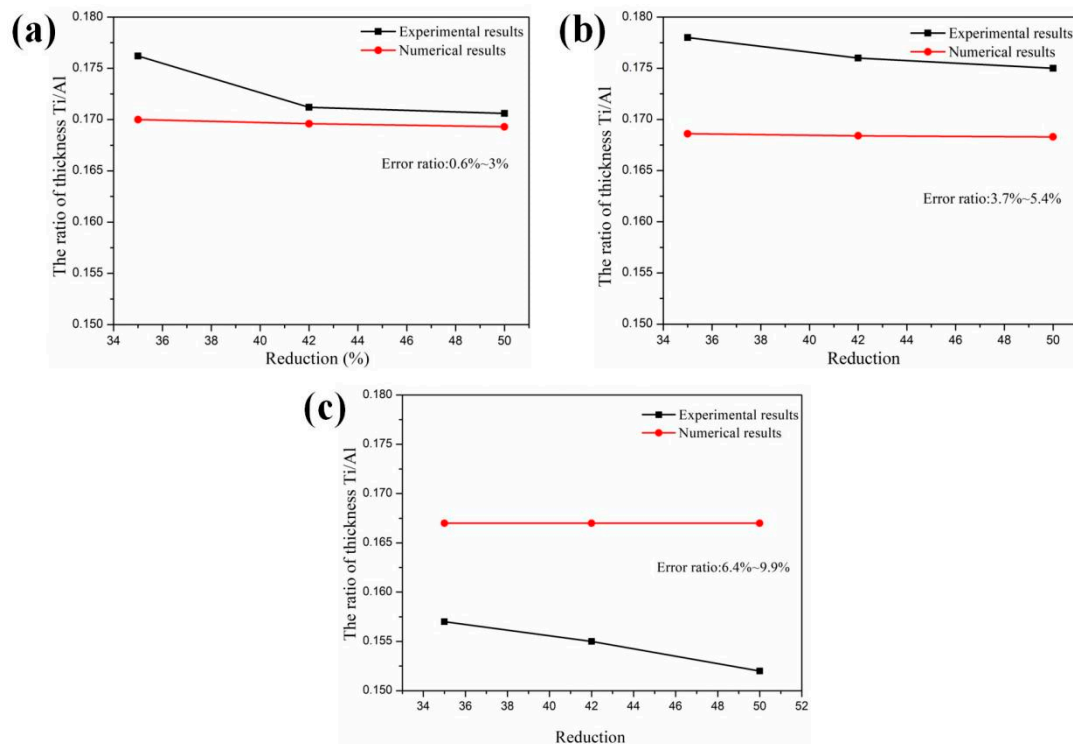


**Figure 8.** Ti/Al thickness ratio values measured using theoretical model and experiment under different aluminum strengths. (a) S1, (b) S2, (c) S3.

### 3.2. Effect of Total Reduction

Figure 9 shows the effect of different total reductions on the stress distribution,  $x_a$ ,  $x_b$  and  $x_n$ , in the deformation zone. The specific parameters have been identified. The contact arc length increases as the total rolling reduction increases, and higher rolling reduction corresponds to greater vertical pressure, which extrudes the bottom metal to form a bonding, which is consistent with the results in references [19,20,24]. As the position gradually tends to exit, the vertical stress increases and reaches a maximum at  $x_n$  and, in region IV, the vertical stress decreases rapidly. Meanwhile, under different reductions, the vertical stress is the same at  $x_a$ , which indicates that the effects of rolling reductions on vertical pressures are the same before the titanium layer yields. Region II is the widest in the deformation zone, which indicates that the covering layer rupture and the underlying metal flowing towards the crack by extrusion is a continuous, stable and relatively long process. With the increase in aluminum strength, the vertical stress in region II increases significantly, which has an important role in promoting the covering layer rupture and the bonding process of the underlying metal. The relative position of  $x_a$ ,  $x_b$  and  $x_n$  in relation to the length of the deformation zone is given on the right-hand side of Figure 9. As the reduction increases,  $x_n/L$  and  $x_b/L$  gradually decrease, which indicates that  $x_n$  and  $x_b$  gradually move away from the entry point, prompting more aluminum to flow towards the outlet, while  $x_a$  increases insignificantly, especially in the case of higher aluminum strength. If there is an intersection point between the  $x_n/L$ -reduction curve and  $x_a/L$ -reduction curve, it means that at a reduction less than that corresponding to the intersection point, the titanium layer of the composite sheet does not yield in the whole deformation zone and the interfacial bonding has not been formed, so the intersection point is said to be the minimum thickness reduction to provide the necessary condition for the atomic metal bond [24]. There is no intersection here, which means that the metal bond has been formed at 35% reduction, and the more sufficient the metal bond is with the increase in aluminum strength.

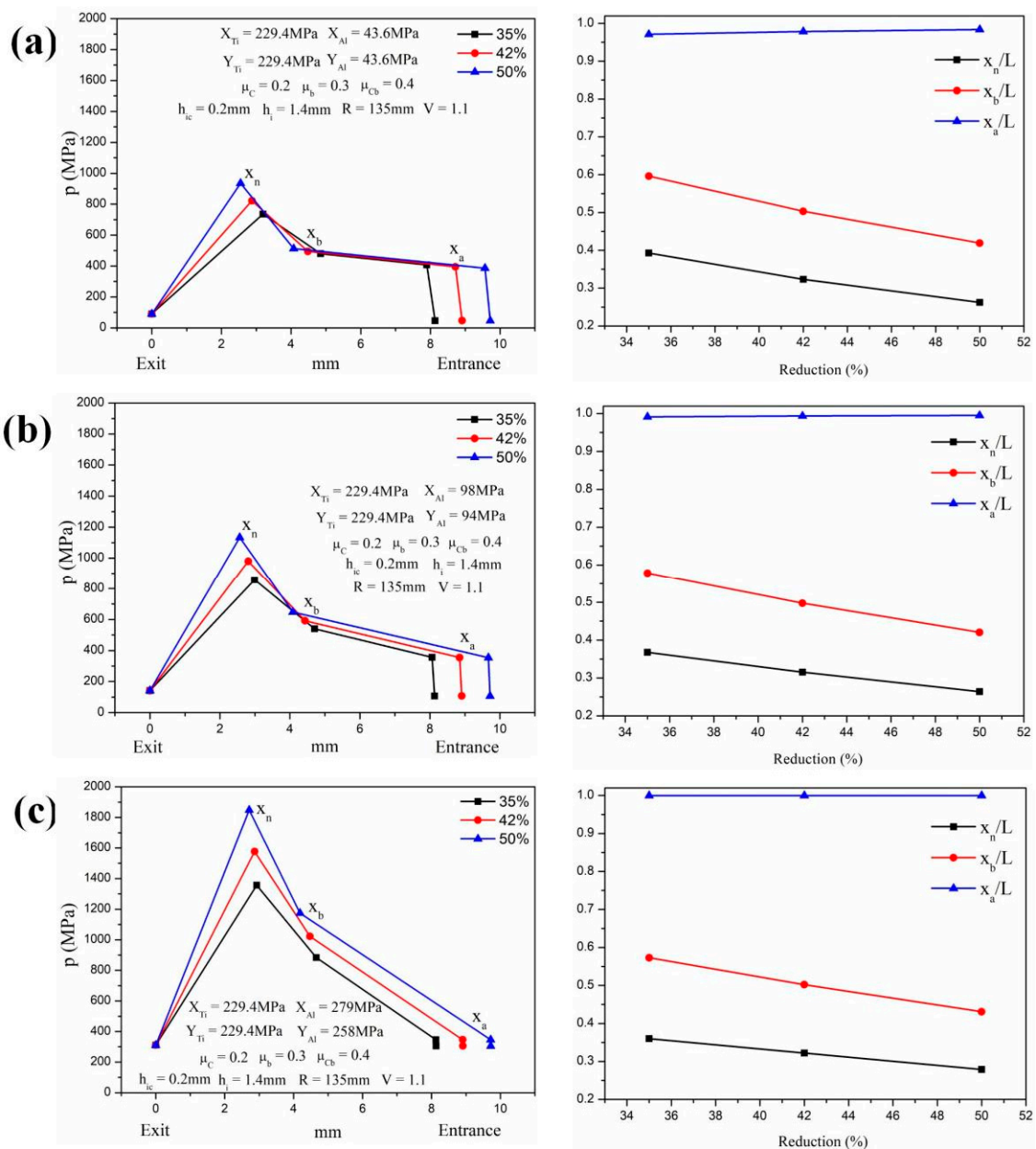


**Figure 9.** Effect of total reductions on the stress distribution,  $x_a$ ,  $x_b$  and  $x_n$ , in the deformation zone. (a) S1, (b) S2, (c) S3.

### 3.3. Effect of Initial Aluminum Strength

Miyajima et al. mentioned, in their article, that by changing the strength of the initial aluminum, the deformation coordination of the Cu/Al laminated composites was significantly improved [26]. On the other hand, the mismatch of the flow stress between the hard layer and soft layer affects the stress distribution and the bonding state. Therefore, using this model, we consider the influence of initial aluminum strength. The effect of initial aluminum strength on the stress distribution,  $x_a$ ,  $x_b$  and  $x_n$ , in the deformation zone is depicted in Figure 10; when the aluminum strength is higher, the vertical stress of the clad sheet in the deformation zone increases, especially in the S3 state. As the aluminum strength increases,  $x_a$  moves towards the entrance and the titanium layer yields over a shorter distance, which facilitates the rapid rupture of the covering layer and buys time for the extrusion flow of the underlying fresh metal, and the increase in  $x_a/L$  is obvious under the condition of a smaller reduction. As the aluminum strength increases, the difference between the vertical stress at the entrance ( $x = L$ ) and  $x_a$  gradually decreases, indicating



that the change in vertical stress in region I becomes smaller. The variation trend of  $x_b$  and  $x_n$  with aluminum strength is related to the reduction. At 35% reduction,  $x_b/L$  and  $x_n/L$  decrease as the aluminum strength increases, and  $x_b$  and  $x_n$  move towards the exit. However, at 50% reduction,  $x_b/L$  and  $x_n/L$  increase slightly, and  $x_b$  and  $x_n$  move to the entrance; the composite plate experiences a relatively short distance before forming a joint. The higher the aluminum strength, the more rapidly the vertical stress increases in region II, and the higher aluminum strength increases the rolling speed of the composite sheet and approaches the roll speed more quickly.

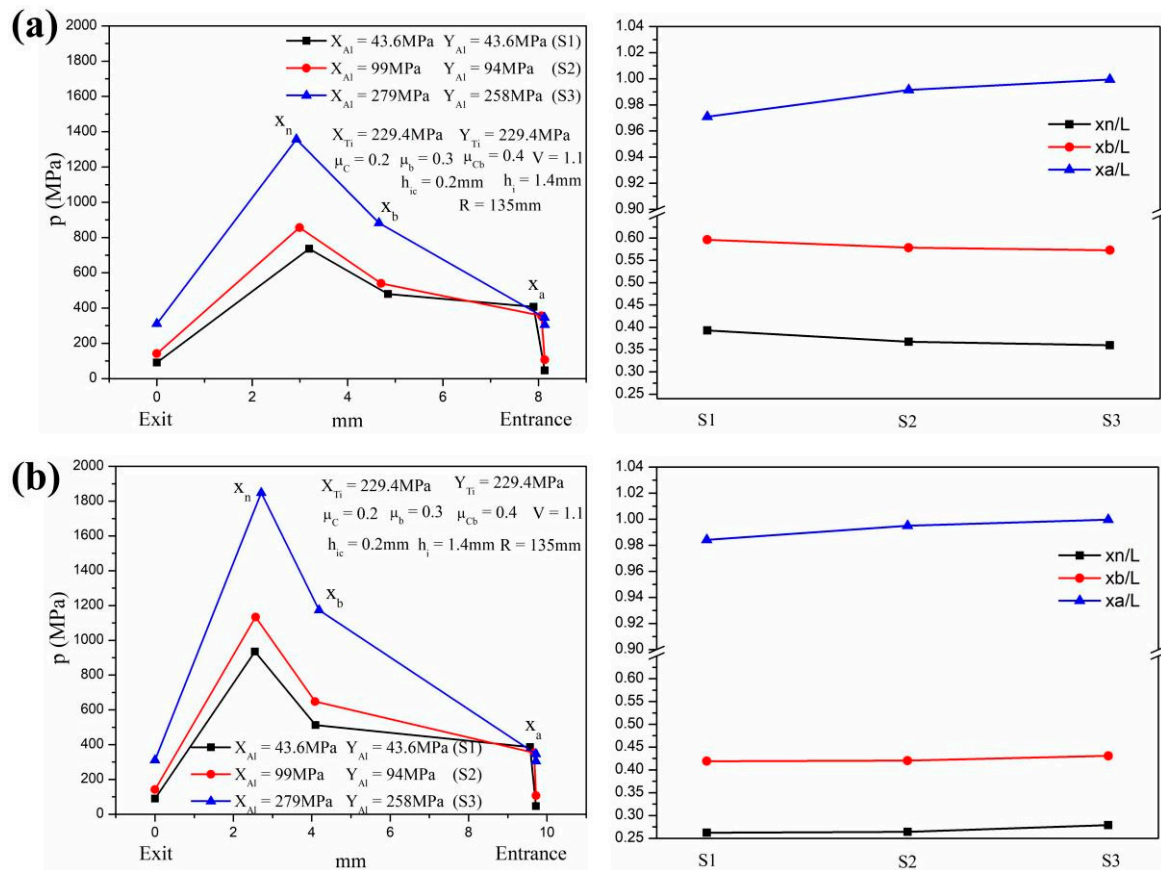


**Figure 10.** Effect of aluminum strength on the stress distribution,  $x_a$ ,  $x_b$  and  $x_n$ , in the deformation zone. (a) Reduction of 35%, (b) reduction of 50%.

It can be seen from Figure 11 that, under the same reduction, the higher the aluminum strength, the better the deformation coordination between the titanium and aluminum layers. Meanwhile, a higher reduction helps the deformation of the titanium and aluminum layers to be coordinated. We know that the more coordinated the deformation of the composite sheet, the more uniform the microstructure in each layer and the more stable the performance of the composite sheet. From the theoretical model calculations, we know that the rolling reduction and the initial aluminum strength are the two key factors to achieve the coordination of the deformation of the composite sheet. At the same time, we have conducted corresponding rolling experiments. Figure 12 shows the deformation of each layer of three types of Ti/Al composite sheets under different rolling reductions. It can be seen that with the increase in rolling reduction, the deformation coordination between the titanium and aluminum layers is better, and with the increase in initial aluminum strength, the deformation coordination is also better. At a 50% reduction rate,  $\epsilon_{Ti}/\epsilon_{Al}$  increases from 93.8% to 98.1%, which is consistent with the trend of the results calculated using this model.

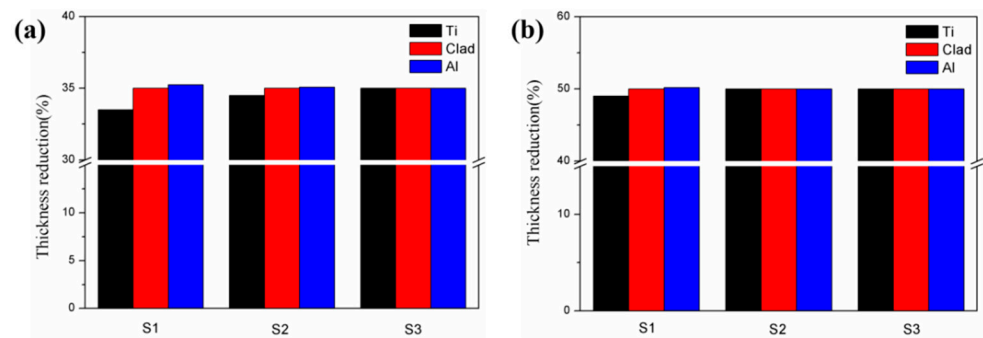


**Figure 11.** Effect of aluminum strength on the deformation of each layer of composite sheet under different reductions calculated using the model. (a) Reduction of 35%, (b) reduction of 50%.

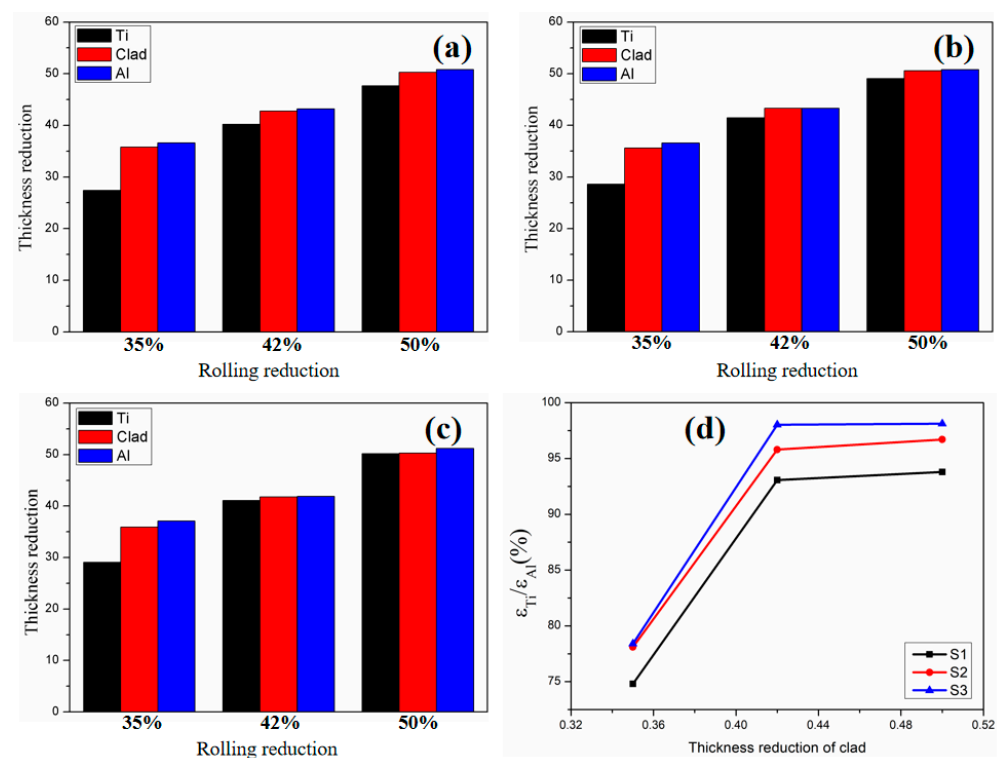


**Figure 12.** Deformation of each layer of three types of Ti/Al composite sheets under different rolling reductions. (a) S1, (b) S2, (c) S3, (d) variation of deformation ratio of titanium and aluminum with total rolling reduction.

### 3.4. Effect of the Coefficient of Friction between Titanium and Aluminum

Different surface treatments will produce different covering layers on the surface of each layer, thus producing different friction coefficients between the faying surfaces of each layer of the composite sheet. Some researchers have shown that wire brushing is more effective than chemical surface treatment in improving the interface bonding performance [27,28]. Therefore, we used wire brushing to treat the surface when conducting experimental verification. The effect of the friction coefficient between titanium and aluminum on the stress distribution and the bonding state in the deformation zone is related to the initial aluminum strength. Since the friction coefficient defined in Section 2.5 is related to the position in the deformation zone, here, we take  $\mu_{cb}$  as the change target, and substitute the change in the overall friction coefficient. As shown in Figure 13a, in the S1 state, the distribution of the vertical stress in region II changes clearly. As  $\mu_{cb}$  increases, the corresponding vertical stress at  $x_a$  becomes smaller, but when the titanium layer yields, the vertical stress increases greatly.  $x_n/L$ ,  $x_b/L$  and  $x_a/L$  increase slightly with increas-



ing  $\mu_{cb}$ . In the S3 state, the increase range of vertical stress in region II becomes larger with the increase in  $\mu_{cb}$ , while the increase range of vertical stress in region III remains constant.  $x_n/L$  and  $x_b/L$  increase greatly with the increase in  $\mu_{cb}$ , while  $x_a/L$  does not change significantly, and  $x_n$  and  $x_b$  gradually move towards the entrance. The larger  $\mu_{cb}$  promotes the formation of the bond closer to the entrance, and the bonded composite sheet experiences a longer distance under higher vertical stress, which contributes to the improvement of the bonding performance, which also confirms that the use of mechanical surface treatment (e.g., wire brushing) has a better effect on improving bonding properties than surface chemical treatments. The vertical stress distribution curves in the deformation zone have a common point for both the S1 and S2 states, that is, the vertical stress varies significantly with the increase in  $\mu_{cb}$  up to the bonding point  $x_b$  (from the inlet to the outlet), which is due to the relative sliding between the titanium and aluminum layers before the bond is formed.

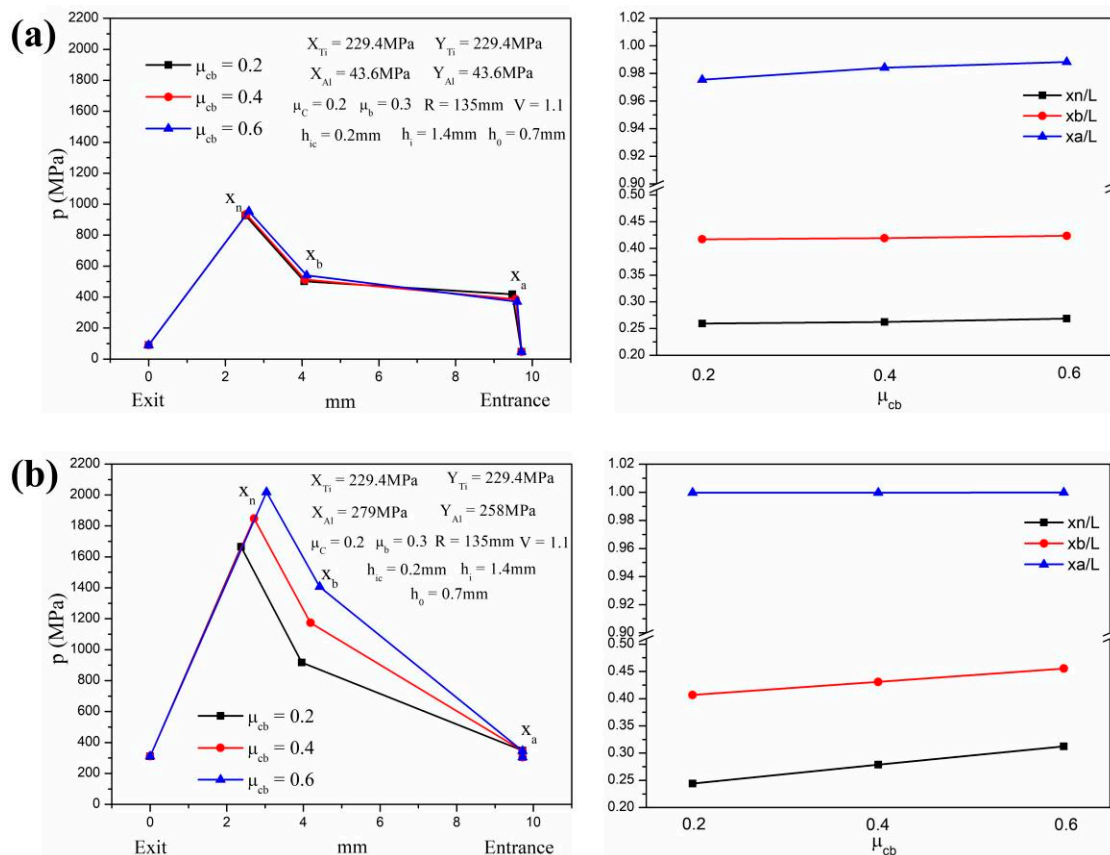


**Figure 13.** Effect of friction coefficient between titanium and aluminum on the stress distribution,  $x_a$ ,  $x_b$  and  $x_n$ , in the deformation zone. (a) S1, (b) S3.

### 3.5. Effect of Initial Thickness of Aluminum Layer

There are certain requirements for the thickness ratio between composite layers in actual service situations. The different thickness ratios will affect the stress distribution and bonding state. The effect of the initial thickness of the aluminum layer on the stress distribution,  $x_a$ ,  $x_b$  and  $x_n$ , in the deformation zone at 50% reduction is illustrated in Figure 14; the thickness of the aluminum layer varies from 0.6 mm to 1.8 mm, and other parameters remain unchanged. As the thickness of the aluminum layer increases, the vertical stress in the deformation zone decreases,  $x_b/L$  and  $x_n/L$  decrease,  $x_a/L$  does not change much and the bonding point  $x_b$  and neutral point  $x_a$  gradually move away from the entrance. The larger the thickness of the aluminum layer, the longer the required distance is for the lower rolling pressure in the deformation zone to extrude the underlying fresh

metal to form a bonding. When the thickness of the aluminum layer is 1.8 mm,  $x_b$  is the farthest distance relative to the entrance. After the formation of the bonding, the vertical stress acting on the interface of the composite sheet is relatively small, the metal flow and mutual embedment near the bonded interface are insufficient and the overall bonding strength is relatively low. Meanwhile, when the thickness of the aluminum layer is 0.6 mm, the vertical stress increases sharply, and the rolling mill is overloaded. Therefore, the most suitable thickness of the aluminum layer here is 1.2 mm.

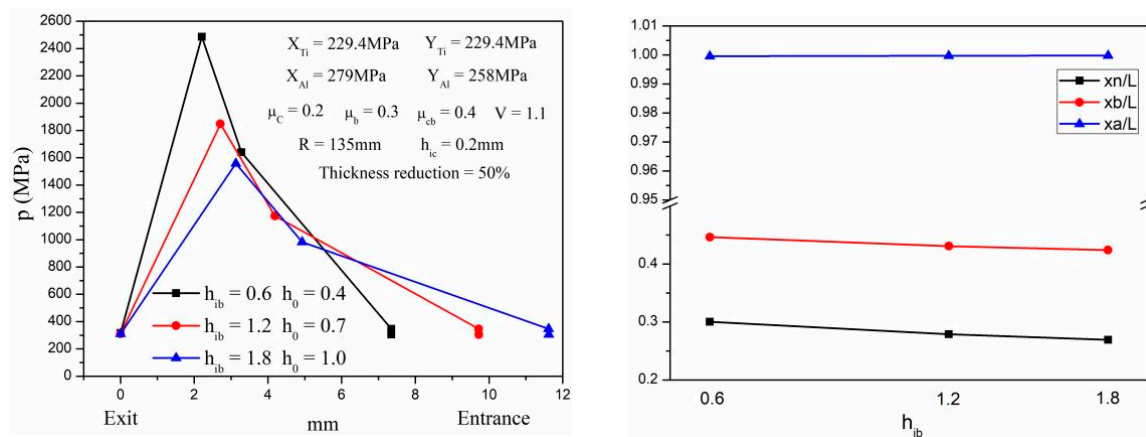


**Figure 14.** Effect of initial thickness of aluminum layer on the stress distribution,  $x_a$ ,  $x_b$  and  $x_n$ , in the deformation zone at 50% reduction.

#### 4. Conclusions

In this work, a Ti/Al cold-rolled deformation model was established using the slab method, which takes into account the anisotropic effect and position-dependent friction model. This model enhances the reliability of the slab method by studying the rolling deformation of layered metal composites. The Ti/Al thickness ratio calculated using the model is consistent with the experimental results, and the maximum error is not more than 10%. The theoretical model results show that with the increase in rolling reduction, the bonding point gradually moves away from the inlet, which promotes more aluminum to flow to the outlet. Meanwhile, the greater vertical stress after the formation of bonding has a catalytic effect on the enhancement of the interfacial bonding properties. The higher the initial aluminum strength, the more coordinated the deformation of the composite sheet and the more stable the properties. Meanwhile, at 50% reduction, the higher the initial aluminum strength and the closer the corresponding bonding point is to the inlet, causing the longer relative distance experienced by the composite sheet under higher rolling pressure after the joint formation, which can promote the improvement of the bonding property, which is consistent with the experimental results. The greater the friction between the titanium and aluminum layers, the more conducive to the improvement of the bonding property. This study can provide a theoretical reference for the design of layered metal composites with large deformation differences.

**Author Contributions:** Conceptualization and Original Draft Preparation, J.L.; Methodology, Q.L. and S.J.; Data Curation, J.W. (Jiang Wu); Review and Editing, F.W. and J.W. (Jiang Wang); Project Administration, X.Z. All authors have read and agreed to the published version of the manuscript.

**Funding:** The authors would like to thank the Science and Technology Base and Talent Special Project of Guangxi Province, China (AD19245030 and AD20325007), the Guangxi University Middle-aged and Young Teachers' Basic Scientific Research Ability Improvement Project, China (2021KY0219), the Guangxi Key Laboratory of Information Materials and Guilin University of Electronic Technology, China (201018Z), and the Hebei Provincial Natural Science Foundation of China (Grant No. E2022209114) for their support.

**Institutional Review Board Statement:** Not applicable.

**Informed Consent Statement:** Not applicable.

**Data Availability Statement:** Not applicable.

**Conflicts of Interest:** The authors declare no conflict of interest.

### Nomenclature

$h_i$	Thickness of the composite sheet before rolling	$\sigma_1, \sigma_2, \sigma_3$	Principal stresses in axial directions
$h_{ic}$	Thickness of Ti layer before rolling	$P$	Vertical pressure
$h_{ib}$	Thickness of Al layer before rolling	$\sigma_c$	Horizontal tensile stress of Ti layer
$h_0$	Thickness of the composite sheet after rolling	$\sigma_b$	Horizontal tensile stress of Al layer
$h_{0c}$	Thickness of the Ti layer after rolling	$\sigma$	Horizontal tensile stress of composite sheet as a whole
$h_{0b}$	Thickness of the Al layer after rolling	$\tau_c$	Friction stress between the upper roll and Ti layer
$h_c$	Height of upper element with respect to horizontal axis	$\tau_b$	Friction stress between the lower roll and Al layer
$h_b$	Height of upper element with respect to horizontal axis	$\tau_{cb}$	Friction stress between the Ti and Al layers
$h$	Height of element as a whole with respect to horizontal axis	$P_c$	Pressure of the upper roll on Ti layer
$R$	Radius of the rolls	$P_b$	Pressure of the lower roll on Al layer
$\omega$	Angular velocity of rolls	$P_{cb}$	Pressure on the contacting surfaces of Ti and Al layers
$L$	Contact arc length	$x_a$	Starting point of the yielding of the Ti layer
$\theta$	Variable contact angle of upper roll	$x_b$	The point at which extrusion of fresh metal from the faying surfaces comes into contact (i.e., the bonding point)
$\theta'$	The tilt angle of the contacting sides of Ti and Al layers	$x_n$	The point where the velocity direction of the composite sheet changes (i.e., the neutral point)
$\gamma$	Variable contact angle of lower roll	$S$	Stress factor

### References

- Xiao, H.; Qi, Z.C.; Yu, C.; Xu, C. Preparation and properties for Ti/Al clad plates generated by differential temperature rolling. *J. Mater. Process. Tech.* **2017**, *249*, 285–290. [\[CrossRef\]](#)
- Li, J.S.; Wang, S.Z.; Mao, Q.Z.; Huang, Z.W.; Li, Y.S. Soft/hard copper/bronze laminates with superior mechanical properties. *Mater. Sci. Eng. A* **2019**, *756*, 213–218. [\[CrossRef\]](#)
- Poddar, V.S.; Rathod, M.J. Evaluation of mechanical properties of cold roll bonded mild steel and aluminum. *Mater. Today Proc.* **2021**, *43*, 1–9. [\[CrossRef\]](#)
- Kim, M.J.; Lee, K.S.; Han, S.H.; Hong, S.I. Interface strengthening of a roll-bonded two-ply Al/Cu sheet by short annealing. *Mater. Charact.* **2021**, *174*, 111021. [\[CrossRef\]](#)
- Vaseghi, M.; Zand, H.; Sameezadeh, M. Mechanical bonding in cold roll-cladding of tri-layered brass/steel/brass composite. *Int. J. Mater. Res.* **2020**, *111*, 826–832. [\[CrossRef\]](#)
- Ebrahimi, M.; Liu, G.P.; Li, C.W.; Wang, Q.D.; Jiang, H.Y.; Ding, W.J.; Su, F.L.; Shang, Z.P. Characteristic investigation of trilayered Cu/Al8011/Al1060 composite: Interface morphology, microstructure, and in-situ tensile deformation. *Prog. Nat. Sci.* **2021**, *31*, 679–687. [\[CrossRef\]](#)
- Ebrahimi, M.; Liu, G.P.; Li, C.W.; Wang, Q.D.; Jiang, H.Y.; Ding, W.J.; Su, F.L. Experimental and numerical analysis of Cu/Al8011/Al1060 trilayered composite: A comprehensive study. *J. Mater. Res. Technol.* **2020**, *9*, 14695–14707. [\[CrossRef\]](#)
- Khaledi, K.; Brepols, T.; Reese, S. A multiscale description of bond formation in cold roll bonding considering periodic cracking of thin surface films. *Mech. Mater.* **2019**, *137*, 103142. [\[CrossRef\]](#)
- Rezaia, A.; Shafieib, E.; Ostovan, F. Experimental & theoretical investigation of roll bonding process of multilayer strips by finite element method. *J. Manuf. Process.* **2020**, *54*, 54–69.
- Khaledi, K.; Rezaei, S.; Wulfinghoff, S.; Reese, S. Modeling of joining by plastic deformation using a bonding interface finite element. *Int. J. Solids Struct.* **2019**, *160*, 68–79. [\[CrossRef\]](#)
- Zhang, R.H.; Liu, J.H.; He, C.H.; Zhao, H.L.; Wang, Q.L. Test and simulation study of the effect of transverse impact stress on the rosette 19-hole gun propellant under low temperature. *FirePhysChem* **2022**, *2*, 147–153. [\[CrossRef\]](#)
- Haghighat, H.; Saadati, P. An upper bound analysis of rolling process of non-bonded sandwich sheets. *Trans. Nonferrous Met. Soc. China* **2015**, *25*, 1605–1613. [\[CrossRef\]](#)
- Maleki, H.; Bagherzadeh, S.; Mollaei-Dariani, B.; Abrinia, K. Analysis of Bonding Behavior and Critical Reduction of Two-Layer Strips in Clad Cold Rolling Process. *J. Mater. Eng. Perform.* **2013**, *22*, 917–925. [\[CrossRef\]](#)

14. Ebrahimi, M.; Nazari Tiji, S.A.; Djavanroodi, F. Upper bound solution of equal channel forward extrusion process as a new severe plastic deformation method. *Metall. Res. Technol.* **2015**, *112*, 609. [[CrossRef](#)]
15. Hwang, Y.M.; Hsu, H.H.; Hwang, Y.L. Analytical and experimental study on bonding behavior at the roll gap during complex rolling of sandwich sheet. *Int. J. Mech. Sci.* **2000**, *42*, 2417–2437. [[CrossRef](#)]
16. Dobronosov, Y.K.; Gavrish, P.A. Investigation of the stress-strain and kinematic state of metal in rolling welded joints between copper and steel. *Weld. Int.* **2017**, *31*, 874–878. [[CrossRef](#)]
17. Salikhyanov, D. Contact mechanism between dissimilar materials under plastic deformation. *CR Mec.* **2019**, *347*, 588–600. [[CrossRef](#)]
18. Parvizi, A.; Afrouz, F. Slab analysis of asymmetrical clad sheet bonded before rolling process. *Int. J. Adv. Manuf. Tech.* **2016**, *87*, 137–150. [[CrossRef](#)]
19. Wang, H.Y.; Li, X.; Sun, J.; Wang, Z.H.; Zhao, D.W.; Zhang, D.H. Analysis of sandwich rolling with two different thicknesses outer layers based on slab method. *Int. J. Mech. Sci.* **2016**, *106*, 194–208. [[CrossRef](#)]
20. Chaudhari, G.P.; Acoff, V. Cold roll bonding of multi-layered bi-metal laminate composites. *Compos. Sci. Technol.* **2009**, *69*, 1667–1675. [[CrossRef](#)]
21. Tzou, G.Y. Theoretical study on the cold sandwich sheet rolling considering Coulomb friction. *J. Mater. Process. Tech.* **2001**, *114*, 41–50. [[CrossRef](#)]
22. Pan, S.C.; Huang, M.N.; Tzou, G.Y.; Syu, S.W. Analysis of asymmetrical cold and hot bond rolling of unbounded clad sheet under constant shear friction. *J. Mater. Process. Tech.* **2006**, *177*, 114–120.
23. Huang, M.N.; Tzou, G.Y.; Syu, S.W. Investigation on comparisons between two analytical models of sandwich sheet rolling bonded before rolling. *J. Mater. Process. Tech.* **2003**, *140*, 598–603. [[CrossRef](#)]
24. Yang, W. *An Investigation of Bonding Mechanism in Metal Cladding by Warm Rolling*; Texas A&M University Press: College Station, TX, USA, 2011.
25. Hill, R. *The Mathematical Theory of Plasticity*. Oxford University Press: Oxford, UK, 1998.
26. Miyajima, Y.; Iguchi, K.; Onaka, S.; Kato, M. Effects of Rolling Reduction and Strength of Composed Layers on Bond Strength of Pure Copper and Aluminium Alloy Clad Sheets Fabricated by Cold Roll Bonding. *Adv. Mater. Sci. Eng.* **2014**, *2014*, 1–11. [[CrossRef](#)]
27. Vaidyanath, L.R.; Milner, D.R. Significance of surface preparation in cold pressure welding. *Br. Weld. J.* **1960**, *7*, 1–6.
28. Zhang, W.; Bay, N. Cold welding-fractographic investigation of the weld formation. *Weld. Res. Suppl.* **1997**, *9*, 361s–366s.

**Disclaimer/Publisher’s Note:** The statements, opinions and data contained in all publications are solely those of the individual author(s) and contributor(s) and not of MDPI and/or the editor(s). MDPI and/or the editor(s) disclaim responsibility for any injury to people or property resulting from any ideas, methods, instructions or products referred to in the content.